```
    FOR iterations 1 to 4
      Compute observation set ρ_c using X̄(t_2)
      Δρ := ρ − ρ_c
      ∂ρ/∂X̄ := ρ̂^T
      Computation of estimated state X̂(t_2) and updating
      of U, D factors using UDU^T sequential estimation
      algorithm
      D := D + Q
      X̄(t_2) := X̂(t_2)
    NEXT ITERATION
    t_1 := t_2
    X̂(t_1) := X̂(t_2)
  END
END
```

Conclusion

By utilizing the range to three active landmarks, an estimation algorithm has been developed to estimate the geodetic satellite position. Simulation results showed that with such a simple model a position determination accuracy of better than 200 m can be achieved. The algorithm porposed is well suited for onboard applications because of its simplicity.

Acknowledgments

We thank Mr. K. N. Srinivasa Murthy for his fruitful suggestions in developing the algorithm, particularly in the area of inclusion of process noise in the estimation algorithm. Our thanks are also due to Mrs. B. P. Dakshayani for the help in providing the various types of simulated observations.

References

[1]Mease, K. D., Ryne, M. S., and Wood, L. J., "An Approach to Autonomous, Onboard Orbit Determination," AIAA Paper 84-2031, Aug. 1984.

[2]Liu, A. S., "Autonomous Satellite Navigation Using the Stellar Horizon Atmospheric Dispersion Sensor," AIAA Paper 83-861, Aug. 1983.

[3]Rene, Z. X., "Autonomous Satellite Navigation and Orbit-Keeping Using Attitude Sensors," IAF-ST-84-12, 35th Congress of the International Astronautical Federation, Lausanne, Switzerland, Oct. 1984.

[4]Hall, D. L. and Waligora, S. R., "Orbit/Attitude Estimation with Landsat 1 and 2 Landmark Data," AAS 79-152, *Astrodynamics 1979, Advances in Astronautical Sciences,* Vol. 40, Pt. 1, pp. 187–211.

[5]Chodas, P., "Application of Extended Kalman Filter to Several Formulations of Orbit Determination," Univ. of Toronto, Toronto, Ontario, Canada, UTIAS TN-224.

[6]Bierman, G. J., "Factorization Methods for Discrete Sequential Estimation," *Mathematics in Science and Engineering*, Vol. 128, Academic, New York, 1977, Chap 5.

Flexible Manipulator Modeling for Control System Development

V. A. Spector* and H. Flashner†
University of Southern California, Los Angeles, California

I. Introduction

WEIGHT limits imposed on space-based systems, such as robots, lead to highly flexible structures. Consequently, compensation for structural flexibility is an important factor in achieving performance specifications.[1-3] High-accuracy endpoint positioning requires direct measurement of end-effector position and possibly of displacements at intermediate locations, thus creating a noncollocated control system. Separating the actuators and sensors creates a delay between control action and sensors measurement, adversely affecting both system stability and performance. Propagation delay in flexible links has been experimentally found[4] to significantly limit control system performance.

In this Note, application of Euler and Timoshenko beam theories to flexible link modeling for control design is examined from several points of view. In addition to transfer functions (gain and phase), frequency-domain wave propagation solutions are obtained for both the Euler and Timoshenko models by using transform techniques. The resulting dispersion equations are analyzed to explain differences between the models and the impact of these differences on factors pertinent to control design, such as time delay. Bounds on the range of validity of Euler theory for control modeling are obtained by comparison of transfer functions with those resulting from Timoshenko theory.

II. Dynamic Equations of Motion

Consider the motion of a rotation beam undergoing a bending deformation $y(x,t)$ and a cross-sectional rotation $\psi(x,t)$. Assuming small motions, the resulting equations of motion are

$$EI\frac{A^2\psi}{\partial x^2} + \kappa GA\left(\frac{\partial y}{\partial x} - \psi\right) - \rho I\frac{\partial^2\psi}{\partial t^2} = 0 \tag{1a}$$

$$\rho A\frac{\partial^2 y}{\partial t^2} - \kappa GA\left(\frac{\partial^2 y}{\partial x} - \frac{\partial\psi}{\partial x}\right) = 0 \tag{1b}$$

where ρ is the mass density, A cross-sectional area, E the Young's modulus, G the shear modulus, κ the Timoshenko shear coefficient, and I the area moment of inertia.

Equations (1) represent the Timoshenko beam model.[5] This model includes both the rotary inertia and shear effects and is the most accurate model that derives from strength of materials. The shear coefficient κ is dimensionless and depends on Poisson's ratio and the shape of the cross section (see Ref. 6).

If both shear and rotary inertia are neglected, the Euler-Bernoulli model results:

$$EI\frac{\partial^4 y(x,t)}{\partial x^4} + \rho A\frac{\partial^2 y(x,t)}{\partial t^2} = 0 \tag{2}$$

III. Solution Methods

To solve the equations of motion, a Laplace transform with s as the time transform variable is taken. The resulting ordinary differential equation for the Laplace transform has the characteristic equation for the Euler-Bernoulli model:

$$p^4 + [(\rho A/EI)]/s^2 = 0 \tag{3}$$

and for the Timoshenko model:

$$p^4 - \frac{\rho}{E}s^2\left(1 + \frac{E}{\kappa G}\right)p^2 + \frac{\rho A}{EI}s^2\left(1 + \frac{\rho I s^2}{\kappa GA}\right) = 0 \tag{4}$$

The solution has the form

$$y(x,s) = \sum_{n=1}^{n=4} C_n(S)e^{p_n x} \tag{5}$$

where the characteristic exponents p_n, $n = 1,2,3,4$ are the roots of Eqs. (3) and (4), respectively. Explicitly, for the Euler-Bernoulli beam

$$p_{1,2} = \pm\left(-\frac{\rho A}{EI}\right)^{1/4} s^{1/2} \tag{6a}$$

Presented as Paper 87-2264, at the AIAA Guidance, Navigation, and Control Conference, Monterey, CA, Aug. 17-19, 1987; received Feb. 8, 1988; revision received June 6, 1988.

*Graduate Student, Department of Mechanical Engineering; currently, Senior Staff Engineer, TRW,

†Assistant Professor, Department of Mechanical Engineering. Member AIAA.

$$p_{3,4} = \pm i\left(-\frac{\rho A}{EI}\right)^{1/4} s^{1/2} \tag{6b}$$

whereas for the Timoshenko model

$$p_{1,2} = \pm\left(\frac{\rho s}{2E}\right)^{1/2}\left\{\left(1+\frac{E}{\kappa G}\right)s + \left[\left(1-\frac{E}{\kappa G}^2\right)s^2 - \frac{4EA}{\rho I}\right]^{1/2}\right\}^{1/2} \tag{7a}$$

$$p_{3,4} = \pm\left(\frac{\rho s}{2E}\right)^{1/2}\left\{\left(1+\frac{E}{\kappa G}\right)s - \left[\left(1-\frac{E}{\kappa G}\right)^2 s^2 - \frac{4EA}{\rho I}\right]^{1/2}\right\}^{1/2} \tag{7b}$$

Since the form of the solution, given by Eq. (5), is the same for both models, the qualitative difference in behavior of the models is completely determined by these roots.

Wave Solution

The characteristic equations given by Eqs. (3) and (4) could also be obtained by assumings a wave-type solution in the equations of motion:

$$y(x,t) = Ce^{(px+st)} \tag{8}$$

Letting $p = ik$ and $s = i\omega$, Eqs. (3) and (4) become dispersion equations relating the time frequency ω and wavenumber k. Note that these dispersion equations have either pure real or pure imaginary roots. The roots of the dispersion equation $k(\omega)$ determine the character of the solution for any given frequency. Specifically, real k results in a propagating wave, and imaginary k results in a decaying wave. The transition between these two qualitatively different types of solutions occurs when $k = 0$. The frequency for which $k(\omega) = 0$ is called the cutoff frequency. From Eq. (3) it is clear that $k = 0$ is a solution only when $\omega = 0$, and therefore the Euler-Bernoulli model has two propagating and two decaying models at all frequencies. For the Timoshenko beam, Eq. (4) shows that $k = 0$ is also a solution for $\omega_c = (\kappa GA/\rho I)^{1/2}$; therefore, a transition from decaying waves to propagating waves occurs at this frequency.

A comparison between the dispersion curves of the Euler-Bernoulli model, the Timoshenko model, and the dispersion curve of the exact Pochhammer frequency equation derived from three-dimensional elasticity theory for a beam with a solid circular cross section is given in Refs. 5 and 7. The comparison shows that the Euler-Bernoulli curve agrees with the exact solution only at very low frequencies. In particular, the imaginary branch of the solution diverges significantly from the exact model even at relatively low frequencies. On the other hand, the agreement between the Timoshenko and exact solution is excellent on both branches up to and beyond the cutoff frequency. The cutoff frequency $\omega_c = (\kappa GA/\rho I)^{1/2}$, where the imaginary loop transitions into a second real branch, marks the frequency at which shear modes propagate.

For a real wavenumber k, the horizontal phase velocity is defined by $c = \omega/k$. It can be shown easily that for the Euler-Bernoulli beam the speed increases without bound, given nonphysical values of speeds for high frequencies. The Timoshenko beam model, on the other hand, has two branches that reach limit velocities at high frequencies. The first branch exists at all frequencies and approaches a speed $(\kappa G/p)^{1/2}$. The second branch starts at the cutoff frequency and approaches a speed of $c_0 = (E/\rho)^{1/2}$. Using the wave approach, the equivalent delay time for a 1-m-long beam was computed as shown in Fig. 1.

IV. Analysis of Rotating Flexible Link

Two pinned-free beams are analyzed: a thin solid rectangular (10×0.277 cm) slab and a thin-walled (0.1 cm) hollow square (10×10 cm). Gain vs frequency of the thin solid beam transfer function from a torquer at the pinned end to the total deflection at $x = 0.8$ was computed. For this case, the Euler-Bernoulli and Timoshenko models remain indistinguishable beyond the 10th modal frequency and the Timoshenko model cutoff frequency is almost 57,000 times the first natural mode of the beam.

Figure 2a shows the gain/frequency plot for the hollow box beam. Divergence between the two models is apparent even at

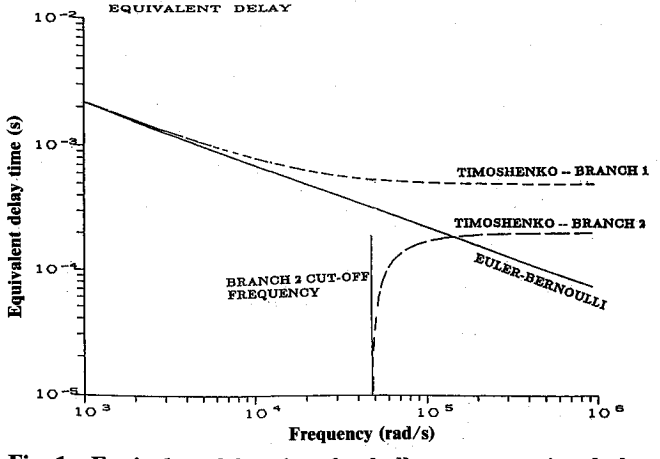

Fig. 1 Equivalent delay time for hollow cross-sectional aluminum beam.

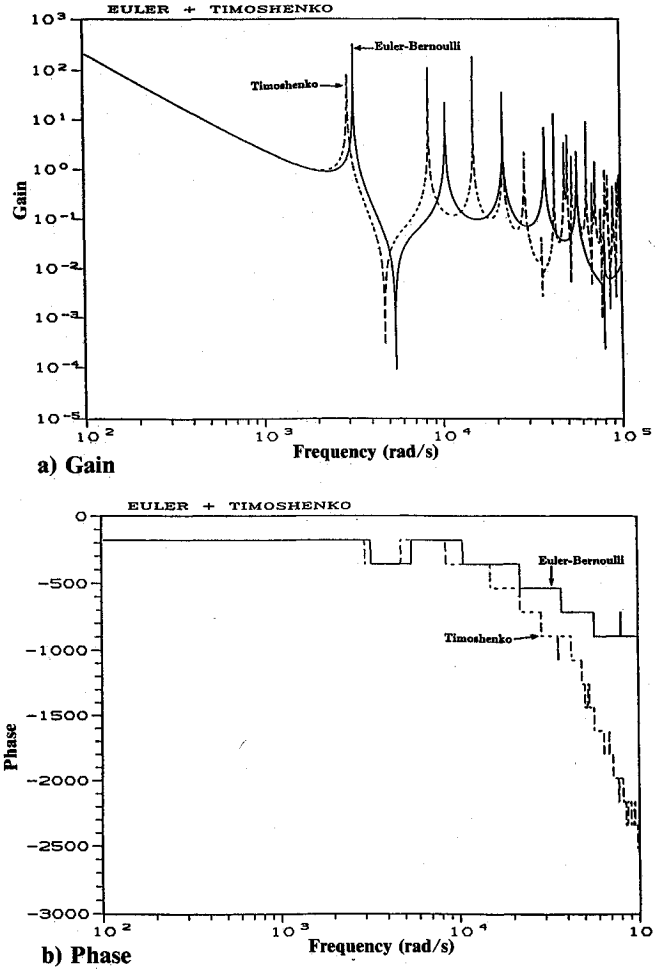

Fig. 2 Transfer function of hollow cross-sectional aluminum beam from torquer to displacement at $x = 0.8$.

the first modal frequency and grows rapidly with frequency. The first three modes differ by 8, 24, and 46%, respectively, with the Timoshenko model predicting consistently lower modal frequencies. Beyond the third mode, the models differ qualitatively, with the Timoshenko model having several modes between every mode of the Euler model. For this cross-section, the ratio between the first natural frequency and the Timoshenko shear mode cutoff frequency is only about 15. The transfer function phase, shown in Fig. 2b, reflects even more clearly the difference between the two models. Phase lag of the Timoshenko model grows at a much greater rate than the Euler-Bernoulli beam. This phase behavior is consistent with delay vs frequency dependence obtained using the wave-solution approach (see Fig. 1). The additional phase lag in the Timoshenko model can be attributed to finite delay at high frequencies, and the Euler model predicts delay approaching zero for high frequencies.

For the same hollow cross section, but constructed of T300 composite, the ratio between the first Euler-Bernoulli model modal frequency and the Timoshenko shear mode cutoff frequency is reduced to only 3.2. As shown in Ref. 7, the divergence between the models is even more severe, with the first Euler-Bernoulli modal frequency 55% higher than the first Timoshenko modal frequency. Beyond the first Euler-Bernoulli modal frequency, the Timoshenko model has several modes for each mode of the Euler-Bernoulli model.

V. Validity of Beam Models

As previously demonstrated, the important parameter in determining the range of validity of the beam models is the shear mode cutoff frequency. The Euler-Bernoulli model is accurate only for frequencies much below (by at least a factor of 20) the cutoff frequency. Use of the Euler-Bernoulli model for control sytsem design is justified only if the control bandwidth is much below the cutoff frequency. A design based on the Euler-Bernoulli model that violates that restriction will result in faulty performance predictions because of overestimation of the modal frequencies. Even worse, closed-loop control instability is likely due to underestimation of the phase lag.

Figure 3 provides normalized curves for determining the validity of the Euler-Bernoulli model for various cross sections. It shows the ratio of shear mode cutoff frequency to first natural frequency as a function of normalized length. For the circular cross sections length is normalized by the cross-sectional radius; for the rectangular cross sections length is normalized to the height of the cross section. For example, a control system designed to control the first bending mode of a beam with a circular shell cross section requires that the length-to-cross-sectional ratio be at least 20 to justify the use of the Euler-Bernoulli model.

The Timoshenko beam model is accurate for frequencies well beyond the shear mode cutoff frequency. This fact can be observed by comparing the dispersion curves of the Timoshenko model and the accurate solution.[5] The first branch of the dispersion curve is within 1% of the exact solution. The second branch of the Timoshenko model starts to diverge noticeably from the exact model only at frequencies 20% higher than the cutoff frequency. Few control problems require bandwidths higher than the cutoff frequency. Hence, in most applications Timoshenko beam model is adequate for control modeling.

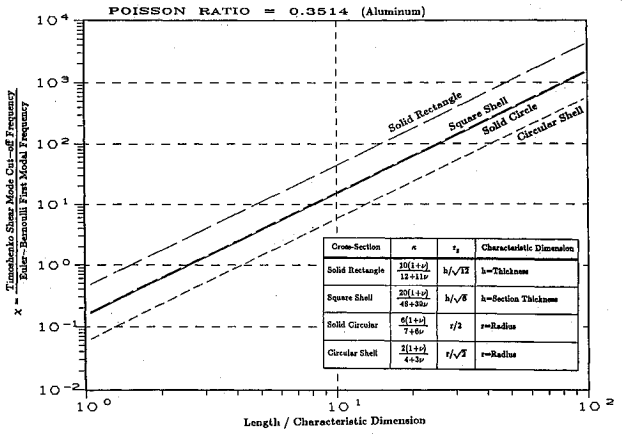

Fig. 3 Normalized curves for determining validity of Euler-Bernoulli beam model.

VI. Conclusions

A study of flexible manipulator link modeling provides quantitative guidelines for determining the range of validity of the frequently used Euler model. Use of the Euler model beyond the range introduces severe errors in the transfer functions required for control analysis. A wave propagation analysis is necessary to interpret the frequency response and calculate the time delay present in a noncollocated control system.

References

[1]Sunada, W. H., and Dubowsky, S., "On the Dynamic Analysis and Behavior of Industrial Robotic Manipulators with Elastric Members," American Society of Mechanical Engineers Paper 82-DET-45, Sept. 1982.

[2]Von Flotow, A. H., "Disturbance Propagation in Structural Networks; Control of Large Space Structures," Ph.D. Thesis, Dept. of Aeronautics and Astronautics, Stanford Univ., Stanford, CA, June 1984.

[3]Wie, B., "On the Modeling and Control of Flexible Space Structures," Guidance and Control Lab., Stanford Univ., Stanford, CA, SUDAAR 525, June 1981.

[4]Cannon, R. H., Jr., and Schmitz, E., "Initial Experiments on the End-Point Position Control of a Flexible One-Link Manipulator," *International Journal of Robotics Research,* Vol. 3, No. 3, Fall 1984, pp. 62–75.

[5]Graff, K. F., *Wave Motion in Elastic Solids,* Ohio State Univ. Press, Columbus, 1975.

[6]Cowper, G. R., "The Shear Coefficient in Timoshenko's Beam Theory," *Journal of Applied Mechanics,* June 1966, pp. 335–340.

[7]Spector, V. A., and Flashner, H., "Flexible Manipulator Modeling in Control System Development," *Proceedings of the AIAA Guidance, Navigation and Control Conference,* AIAA, New York, 1987, pp. 213–220.

Tracking with Paired Angle Measurement Sensors

Thomas R. Blackburn*
McDonnell Douglas Space Systems Company, Huntington Beach, California

Nomenclature

$\boldsymbol{d}$	= target line-of-sight unit direction vector
E	= assumed energy level
$\boldsymbol{H}$	= observation vector sensitivity to state vector change matrix
h	= transformation from the trajectory state to the observation vector
$\boldsymbol{p}_S, \boldsymbol{p}_T$	= sensor and target position vectors, respectively
$\boldsymbol{R}$	= observation vector noise covariance matrix, or the distance from Earth's center, as appropriate

Received May 9, 1988; revision received July 28, 1988.

*Manager, Guidance and Navigation.